solids

MDPI

Article

Luminous Transmittance and Color Rendering Characteristics of Evaporated Chalcopyrite Thin Films for Semitransparent Photovoltaics

Cecilia Guillén

Centro de Investigaciones Energéticas Medioambientales y Tecnológicas (CIEMAT), Avda. Complutense 40, 28040 Madrid, Spain; c.guillen@ciemat.es

Abstract: The luminous transmittance and the color rendering index of daylight through semitransparent photovoltaic glazing are essential parameters for visual comfort indoors, and they must be considered for different absorber materials that were traditionally developed for opaque solar cells, such as those of the chalcopyrite type. With this aim, various chalcopyrite compounds ($CuInSe_2$, $CuInS_2$ and $CuGaS_2$) were prepared by means of evaporation and then measured to obtain their optical absorption spectra. These experimental data are used here to calculate the solar absorptance (α_S), luminous transmittance (τ_L) and color rendering index (R_a) as a function of the chalcopyrite film thickness. The comparative analysis of the different factors indicates that 70 nm thick $CuInSe_2$ is optimal to guarantee excellent visual comfort (τ_L = 50% and R_a = 93%) while absorbing as much solar irradiance (α_S = 37%) as 130 nm thick $CuInS_2$ or 900 nm thick $CuGaS_2$. The second option (130 nm thick $CuInS_2$) is also considered good (τ_L = 40% and R_a = 80%), but for $CuGaS_2$, the thickness should be kept below 250 nm in order to obtain a suitable color rendering $R_a \geq 60\%$.

Keywords: semiconductor films; optical absorption; luminous transmittance; color rendering

Citation: Guillén, C. Luminous Transmittance and Color Rendering Characteristics of Evaporated Chalcopyrite Thin Films for Semitransparent Photovoltaics. *Solids* **2024**, *5*, 98–109. https://doi.org/10.3390/solids5010007

Academic Editor: Daniela S. Gogova

Received: 18 December 2023
Revised: 5 February 2024
Accepted: 6 February 2024
Published: 8 February 2024

1. Introduction

In addition to the opaque solar cells used for conventional installations in photovoltaic plants or buildings roofs, new semitransparent photovoltaic systems are being developed for applications in skylights and windows [1,2]. Semitransparent cells are designed to convert a portion of the solar irradiance into electricity while transmitting the remaining sunlight into the building. They can also reduce the cooling load in summer by reducing radiation indoors while maintaining visible comfort [3].

Among the various semiconductor materials that can act as photovoltaic absorbers, compounds with a chalcopyrite structure such as $CuInSe_2$, $CuGaSe_2$ and $CuIn_{1-x}Ga_xSe_2$ have demonstrated long-term stability and high conversion efficiencies at low manufacturing costs [4,5]. The analogous sulfide chalcopyrites, $CuInS_2$ and $CuGaS_2$, are now of renewed interest due to their broader bandgap, which make them good candidates for semitransparent devices [6–8]. Also, the newly discovered wurtzite (cation-disordered) polytype of $CuInS_2$ [9], as well as the wurtzite $ZnSnN_2$ [10] and mixed $ZnSnN_2$ (cation-ordered and -disordered phases) [11], all have similar absorption coefficient values. The chalcopyrite absorbers are commonly prepared as thin films on glass substrates [4,7], because their high absorption coefficient (~10^4 cm^{-1}) allows a low thickness (~1 μm) to be used to absorb the radiation energy greater than the bandgap [12]. Therefore, semitransparency can be straightforwardly achieved by growing thinner chalcopyrite layers below the absorption length in the visible spectral range [13], resulting in less material consumption and reduced deposition time as additional advantages [12,13]. Considering that the maximum photovoltaic conversion efficiency is 23% for chalcopyrite semiconductors with 2.0 μm thickness [12], high efficiencies of around 8% have also been reported for a thickness of 200 nm [12] and 3% for a thickness of 50 nm [13].

Solar radiation undergoes various absorptions in the Earth's atmosphere, and the average energy falling on the Earth's surface at air-mass 1.5 (AM1.5) is the standard spectrum applied to test the conversion efficiency of photovoltaic cells [4,12], which is used here to determine the solar absorptance (α_S). On the other hand, for transparent and semitransparent building elements, European directives define luminous transmittance (τ_L) [14] and colorimetric calculations [15] based on the standard illuminant D65, which represents the typical spectral distribution of daylight in clear conditions at around noon [16]. It should be noted that luminous transmittance takes into account the eye's sensitivity to different wavelengths through standard photopic vision (V) [14], and a value of τ_L~10% is considered sufficient to obtain a comfortable soft daylight effect [2,17]. The product of the conversion efficiency and the luminous transmittance is a single compound parameter called light utilization efficiency (LUE) [18], which allows the comparison of different semitransparent solar cells.

The color perception is another parameter to consider, because in most cases the optical transmittance in the visible wavelength region is not uniform. The correlated color temperature (CCT) and average color rendering index (R_a) are the two main criteria for evaluating whether the natural light transmitted through glazing provides aesthetic comfort [19]. CCT is the temperature of a black-body radiator that has the closest chromaticity to the illuminant (a light source alone or through a transparent medium), allowing the interior light to be distinguished in neutral (3000 K $\leq$ CCT $\leq$ 5000 K), bluish white (CCT > 5000 K) or yellowish white (CCT < 3000 K) [20]. Furthermore, R_a describes quantitatively how accurately the test light reproduces the color of a given object with respect to a perfect reference illuminant [15]. Although, in a strict sense, R_a can only be compared for two illuminants that have the same CCT, in practice, R_a values are also given with respect to a single reference (usually the standard D65), because this provides direct information about the indoor illumination through semitransparent glasses that correspond to different CCTs [19,20]. In any case, an index of 60% $\leq R_a \leq$ 79% is considered good color rendering and $R_a \geq$ 80% is considered excellent [18,21].

In the present work, the optical absorption coefficients of various chalcopyrite thin films ($CuInSe_2$, $CuInS_2$ and $CuGaS_2$ grown by evaporation) were analyzed to test their suitability to be applied in semitransparent photovoltaic glazing. The solar absorptance, luminous transmittance and color rendering index were determined and then combined into a single parameter (a new figure of merit) that was calculated for each chalcopyrite compound based on the respective thickness. This allows for a better evaluation of visual comfort and explores the possibility of reducing material consumption by comparing the optimal absorber thickness for each compound. The correlated color temperature of the transmitted light is linked to the color rendering index and is therefore implicitly included in the figure of merit.

2. Materials and Methods

Chalcopyrite $CuInSe_2$, $CuInS_2$ and $CuGaS_2$ thin films were prepared by means of modulated flux deposition in a custom-designed vacuum chamber [22]. Within the chamber, a rotating holder span soda-lime glass substrates at 30 rpm for evaporation induced by Cu, In, and Ga beam sources, heating to 350 °C by halogen lamps, and a reaction with vapor from elemental Se or S sources in every rotation. All of the base materials were pellets with 99.99% purity. The metals (Cu, In, Ga) were evaporated from shuttered molecular beam effusion cells, which consisted of a water-refrigerated Mo case with a PBN crucible liner surrounded by a heating filament. The chalcogens (Se, S) were evaporated from two-stage Pyrex glass cells with an intermediate valve that separated the evaporating and cracking stages, which could be set at different temperatures. Flux control of all sources was achieved using Eurotherm 902 temperature controllers.

The structural, morphological and optical properties of these films were analyzed in a previous work [23], where the surface morphology was examined via atomic force microscopy (AFM) with a Park XE-100, and the tetragonal chalcopyrite structure was iden-

tified by means of X-ray diffraction (XRD) performed in a Philips X'pert instrument with radiation CuKα (λ = 1.54056 Å) and a Bragg–Brentano θ–2θ configuration. Figure 1a shows representative AFM images and Figure 1b displays the diffraction patterns corresponding to 600 nm thick films, where all the peaks are indexed according to the standard powder diffraction files for chalcopyrite $CuInSe_2$ (card file no. 40-1487), $CuInS_2$ (no. 27-0159), or $CuGaS_2$ (no. 25-0279), without secondary phases.

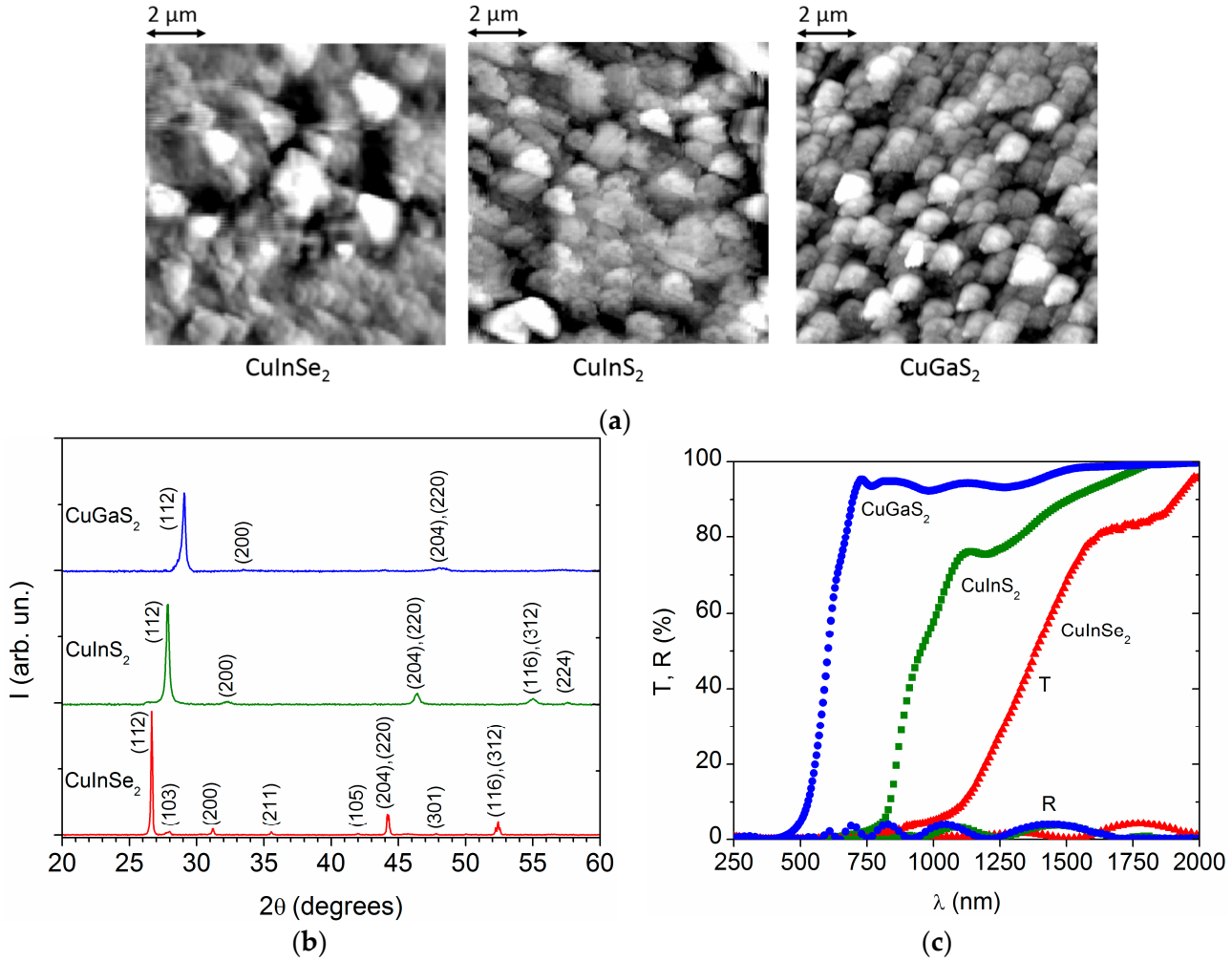

Figure 1. (**a**) AFM images, (**b**) XRD patterns, and (**c**) transmittance and reflectance spectra for evaporated $CuInSe_2$, $CuInS_2$ and $CuGaS_2$ films with 600 nm thickness [23].

The transmittance (T) and reflectance (R) of these chalcopyrite layers are represented in Figure 1c, which were measured with a double beam spectrophotometer Perkin-Elmer Lambda 9, taking the glass substrate as a reference (T_{glass} = 100% and R_{glass} = 0%). Then, the optical absorption coefficient was calculated as follows [24]:

$$\alpha(\lambda) = (1/t)\ \ln\ [1/T(\lambda)] \quad (1)$$

including film thickness (t = 600 nm for the samples in Figure 1).

The optical absorption coefficients were obtained for specific thickness and transmittance values and then extrapolated to obtain the spectra of transmittance and absorptance [12] for different film thicknesses:

$$T(\lambda) = e^{-\alpha(\lambda)t} \quad (2)$$

$$A(\lambda) = 1 - e^{-\alpha(\lambda)t} \quad (3)$$

This calculated spectra are used in Section 3 to evaluate the solar absorptance, as well as the luminous transmittance and color rendering properties of chalcopyrite $CuInSe_2$, $CuInS_2$ and $CuGaS_2$ depending on their respective thickness.

2.1. Determination of the Solar Absorptance and Luminous Transmittance

For each compound and thickness value, the solar radiation that can be collected is given by the product of the standard AM1.5 irradiance (S) and the chalcopyrite absorptance (A) at each wavelength [18]. The photovoltaic performance is thus related to the solar absorptance (α_S), defined as the percentage of the total solar irradiance that is absorbed in the film:

$$\alpha_S = \frac{\sum_{\lambda=250\ nm}^{2500\ nm} A(\lambda)S(\lambda)\Delta\lambda}{\sum_{\lambda=250\ nm}^{2500\ nm} S(\lambda)\Delta\lambda} \quad (4)$$

On the other hand, the luminous transmittance (τ_L) denotes the fraction of the incident light coming from the D65 illuminant that is transmitted by the glazing and is viewed by a standard photopic observer V [14]:

$$\tau_L = \frac{\sum_{\lambda=380\ nm}^{780\ nm} T(\lambda)D65(\lambda)V(\lambda)\Delta\lambda}{\sum_{\lambda=380\ nm}^{780\ nm} D65(\lambda)V(\lambda)\Delta\lambda} \quad (5)$$

where $T(\lambda)$ is the chalcopyrite transmittance.

2.2. Determination of the Correlated Color Temperature

According to the International Commission of Illumination (CIE) [15], the tristimulus values XYZ (in the 1931 CIE color system) indicate how much red, blue and green an illumination source contains. In this work, these contents were calculated for the transmitted light from the standard D65 illuminant, with the color matching functions (R, G and B) shown in Figure 2a, as follows:

$$X_t = \sum_{\lambda=380\ nm}^{780\ nm} T(\lambda)D65(\lambda)R(\lambda)\Delta\lambda \quad (6a)$$

$$Y_t = \sum_{\lambda=380\ nm}^{780\ nm} T(\lambda)D65(\lambda)G(\lambda)\Delta\lambda \quad (6b)$$

$$Z_t = \sum_{\lambda=380\ nm}^{780\ nm} T(\lambda)D65(\lambda)B(\lambda)\Delta\lambda \quad (6c)$$

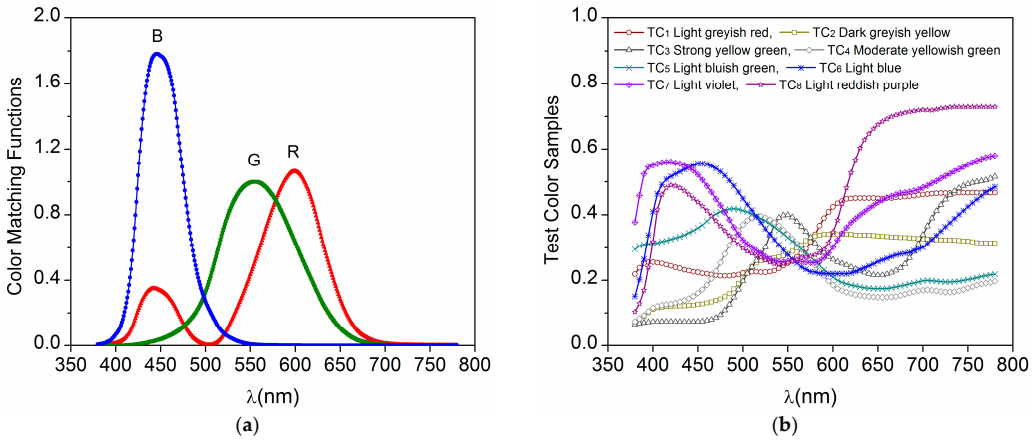

Figure 2. (**a**) Color matching functions and (**b**) test color samples defined by the International Commission on Illumination (CIE) [15], which were used for the various XYZ calculations.

Next, the dimensionless chromaticity coordinates x and y (1931 CIE) for the transmitted light were calculated:

$$x_t = \frac{X_t}{X_t + Y_t + Z_t} \tag{7a}$$

$$y_t = \frac{Y_t}{X_t + Y_t + Z_t} \tag{7b}$$

$$n = \frac{x_t - 0.3320}{0.1858 - y_t} \tag{8}$$

and the correlated color temperature given by [19]:

$$CCT(K) = 449n^3 + 3525n^2 + 6823.3n + 5520.33 \tag{9}$$

Likewise, the reference values are:

$$X_r = \sum_{\lambda=380\ nm}^{780\ nm} D65(\lambda)R(\lambda)\Delta\lambda \tag{10a}$$

$$Y_r = \sum_{\lambda=380\ nm}^{780\ nm} D65(\lambda)G(\lambda)\Delta\lambda \tag{10b}$$

$$Z_r = \sum_{\lambda=380\ nm}^{780\ nm} D65(\lambda)B(\lambda)\Delta\lambda \tag{10c}$$

This resulted in X_r = 95.047, Y_r = 100, Z_r = 108.883, which give x_r = 0.3127, y_r = 0.3290 and CCT = 6504 K for the standard D65 reference.

2.3. Determination of the Color Rendering Index

For color rendering evaluation according to CIE directives [15], we needed to calculate the tristimulus values of the light transmitted by the chalcopyrite film for each of the eight test colors (TC_i, with i = 1 to 8), as shown in Figure 2b:

$$X_{t,i} = \sum_{\lambda=380\ nm}^{780\ nm} TC_i(\lambda)T(\lambda)D65(\lambda)R(\lambda)\Delta\lambda \tag{11a}$$

$$Y_{t,i} = \sum_{\lambda=380\ nm}^{780\ nm} TC_i(\lambda)T(\lambda)D65(\lambda)G(\lambda)\Delta\lambda \tag{11b}$$

$$Z_{t,i} = \sum_{\lambda=380\ nm}^{780\ nm} TC_i(\lambda)T(\lambda)D65(\lambda)B(\lambda)\Delta\lambda \tag{11c}$$

Next, the uniform color space coordinates u and v (1960 CIE) for the transmitted light were calculated:

$$u_{t,i} = \frac{4X_{t,i}}{X_{t,i} + 15Y_{t,i} + 3Z_{t,i}} \tag{12a}$$

$$v_{t,i} = \frac{6X_{t,i}}{X_{t,i} + 15Y_{t,i} + 3Z_{t,i}} \tag{12b}$$

Likewise, $u_{r,i}$ and $v_{t,i}$ were calculated from the reference coordinates:

$$X_{r,i} = \sum_{\lambda=380\ nm}^{780\ nm} TC_i(\lambda)D65(\lambda)R(\lambda)\Delta\lambda \tag{13a}$$

$$Y_{r,i} = \sum_{\lambda=380\ nm}^{780\ nm} TC_i(\lambda)D65(\lambda)G(\lambda)\Delta\lambda \tag{13b}$$

$$Z_{r,i} = \sum_{\lambda=380\ nm}^{780\ nm} TC_i(\lambda)D65(\lambda)B(\lambda)\Delta\lambda \quad (13c)$$

Furthermore, Equation (6a–c) produce (u_t, v_t) values that depend on the chalcopyrite transmittance and Equation (10a–c) provide $u_r = 0.1978$ and $v_r = 0.2967$ for the standard D65 illuminant.

The adaptive color shift was then applied to compensate for the color appearance deviation of each test color sample illuminated under test and reference illuminants, defined as follows:

$$c_{t,i} = \frac{1}{v_{t,i}}(4 - u_{t,i} - 10v_{t,i}) \quad (14a)$$

$$d_{t,i} = \frac{1}{v_{t,i}}(1.708v_{t,i} + 0.404 - 1.481u_{t,i}) \quad (14b)$$

and the coordinates:

$$u'_{t,i} = \frac{10.872 + 0.404c_r\frac{c_{t,i}}{c_t} - 4d_r\frac{d_{t,i}}{d_t}}{16.518 + 1.481c_r\frac{c_{t,i}}{c_t} - d_r\frac{d_{t,i}}{d_t}} \quad (15a)$$

$$v'_{t,i} = \frac{5.520}{16.518 + 1.481c_r\frac{c_{t,i}}{c_t} - d_r\frac{d_{t,i}}{d_t}} \quad (15b)$$

For the standard D65: $c_r = 2.8150$, $d_r = 2.0823$, $u'_t = u'_r = 0.1978, v'_t = v'_r = 0.2967$.

After considering the adaptive color shift, the colorimetric data were transformed according to the 1964 CIE system as follows:

$$W^*_{t,i} = 25(Y_{t,i})^{1/3} - 17 \quad (16a)$$

$$U^*_{t,i} = 13W^*_{t,i}(u'_{t,i} - 0.1978) \quad (16b)$$

$$V^*_{t,i} = 13W^*_{t,i}(v'_{t,i} - 0.2967) \quad (16c)$$

The difference in rendering of a test color sample illuminated directly by the reference illuminant and by the same illuminant transmitted through the chalcopyrite film was quantified as follows:

$$\Delta E_i = \sqrt{\left(U^*_{t,i} - U^*_{r,i}\right)^2 + \left(V^*_{t,i} - V^*_{r,i}\right)^2 + \left(W^*_{t,i} - W^*_{r,i}\right)^2} \quad (17)$$

$$R_i = 100 - 4.6\Delta E_i \quad (18)$$

Finally, the average color rendering index for the eight test colors was

$$R_a = \frac{1}{8}\sum_{i=1}^{8} R_i \quad (19)$$

3. Results and Discussion

All the evaporated chalcopyrite films have high absorption coefficients within the visible spectral range, especially at wavelengths $\lambda < 600$ nm or energies $E > 2.07$ eV, as represented in Figure 3. Compared to $CuGaS_2$, the absorption extends towards the near infrared region for $CuInS_2$ and further for $CuInSe_2$ due to the difference in bandgap energy (E_g) for each material [25]. Although the representation of α vs. E is the most used, Figure 3 shows the dependence of α vs. λ (being $E = hc/\lambda$) to better illustrate the subsequent calculations that are made in terms of wavelengths. In the high absorption region ($\alpha > 10^4$ cm^{-1}), the experimental data show a good fit to the expression that corresponds to direct transitions for polycrystalline semiconductors [26]:

$$\alpha_1 \propto [(\lambda_g - \lambda)/\lambda]^{1/2} \quad (20)$$

giving the gap wavelength λ_g = 560 nm for $CuGaS_2$, λ_g = 870 nm for $CuInS_2$ and λ_g = 1220 nm for $CuInSe_2$, in good agreement with the literature, which establishes direct transitions for chalcopyrite compounds [25,27,28]. The presence of some absorption at $\lambda > \lambda_g$ (or $E < E_g$) is due to tail states that are also typical of chalcopyrite materials [29]. In this other region, the absorption coefficient can be fitted to the form

$$\alpha_2 \propto \exp\{-(\lambda - \lambda_t)^2/2\lambda^2\sigma^2\} \quad (21)$$

where λ_t is a characteristic transition wavelength and σ represents the width of the tail [30,31]. When plotted in wavelengths, the tail width appears larger for $CuInSe_2$ than for $CuInS_2$ and $CuGaS_2$, but when expressed in energy, the width is similar for all three compounds, σ~60 meV, in the same order reported for analogous photovoltaic absorbers [32]. The tail wavelength is found at λ_t = 610 nm for $CuGaS_2$, λ_t = 960 nm for $CuInS_2$ and λ_t = 1350 nm for $CuInSe_2$, slightly above the respective gap wavelength.

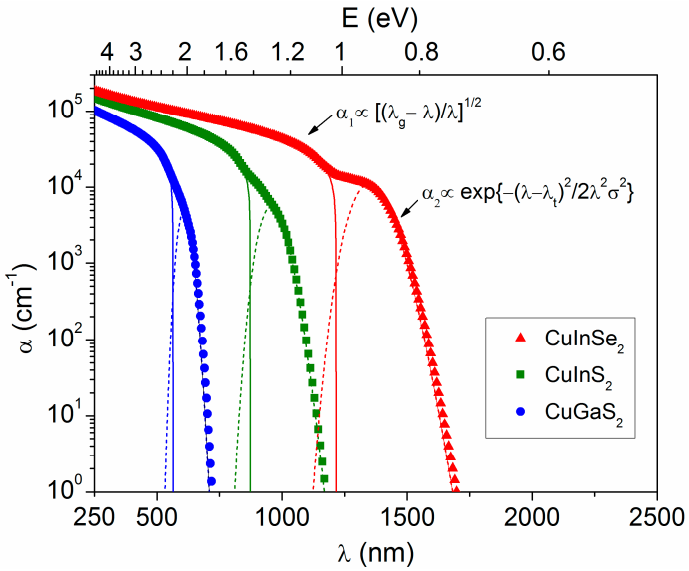

Figure 3. Optical absorption coefficient (α) as a function of radiation wavelength (λ), calculated for the $CuInSe_2$, $CuInS_2$ and $CuGaS_2$ thin films presented in Figure 1. For each sample, the fits used to obtain the wavelength corresponding to the band gap (λ_g) and the band tail (λ_t) are depicted by solid and dashed lines, respectively.

The incident solar irradiance is illustrated in Figure 4a for the standard AM1.5, which has an integrated value $\sum_{\lambda=250\ nm}^{2500\ nm} S(\lambda)\Delta\lambda$ =993 W/m^2, being 4% in the ultraviolet region (λ = 250–380 nm), 53% in the visible region (λ = 380–780 nm), and 43% in the near infrared region (λ = 780–2500 nm) [33]. Figure 4a also includes the absorptance spectra corresponding to 450 nm thick chalcopyrite films in order to compare the optical characteristics of the different compounds with the solar irradiance. Moving on to a quantitative evaluation, Figure 4b represents the percentage of total solar irradiance that is absorbed by each chalcopyrite compound, calculated from Equation (4) depending on the film thickness. The solar absorptance increases quickly with the thickness up to t~450 nm, at which point a value of α_S = 26% is obtained for $CuGaS_2$, α_S = 62% for $CuInS_2$ and α_S = 82% for $CuInSe_2$. However, the increment for each compound is only about 6% from t = 450 nm to t = 900 nm. On the other hand, a value of α_S = 26% is obtained for 80 nm thick $CuInS_2$ and 45 nm thick $CuInSe_2$. The comparative analysis indicates that 70 nm thick $CuInSe_2$ absorbs as much solar irradiance (α_S = 37%) as 130 nm thick $CuInS_2$ and 900 nm thick $CuGaSe_2$.

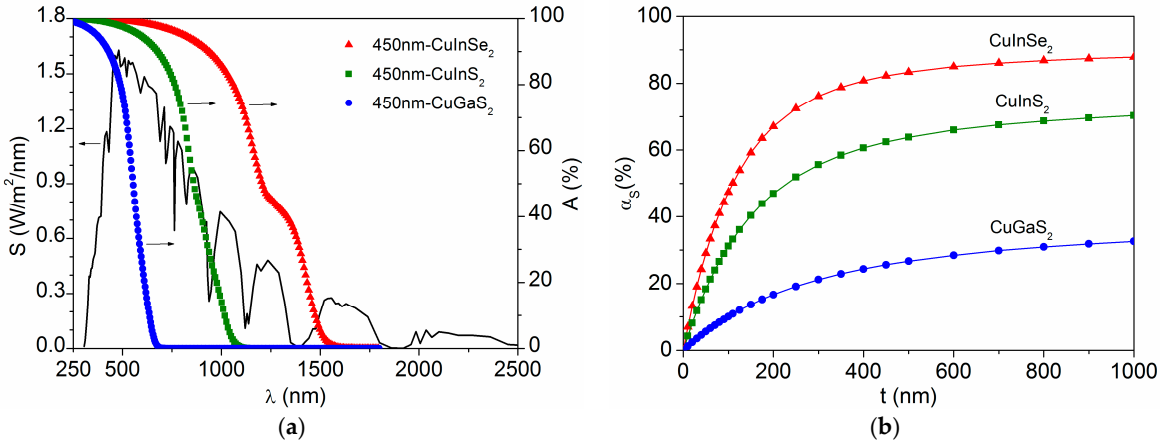

Figure 4. (**a**) Comparison of the standard AM1.5 solar irradiance (S) with the spectral absorptance of 450 nm thick chalcopyrite films, and (**b**) solar absorptance (α_S) for each chalcopyrite compound as a function of the respective thickness.

The spectral distribution of the standard illuminant D65 and standard photopic vision V are represented in Figure 5a, along with the transmittance spectra corresponding to several chalcopyrite thin films for comparison. All of these spectra are used to calculate the luminous transmittance according to Equation (5) for the different chalcopyrite compounds, which is plotted in Figure 5b as a function of the respective film thickness. While reference D65 covers the entire visible region, photopic vision is restricted to the small range where the human eye has sensitivity [34], with a maximum centered at λ_V = 550 nm. Therefore, τ_L is actually given by the transmittance values in a very narrow region around λ_V, although the average transmittance over the whole visible range may be different. For $CuInSe_2$ and $CuInS_2$, the luminous transmittance decreases quickly with the film thickness, being $\tau_L < 10\%$ for $t \geq 300$ nm and $\tau_L < 1\%$ for $t \geq 600$ nm, with $\tau_L = 40\%$ for 90 nm thick $CuInSe_2$ and 130 nm thick $CuInS_2$. Meanwhile, for $CuGaS_2$, the luminous transmittance remains high, even with thicker layers (τ_L = 29% for t = 900 nm). The same value of τ_L = 50% is obtained for 450 nm thick $CuGaS_2$, 100 nm thick $CuInS_2$ and 70 nm thick $CuInSe_2$, but they have different transmittance distributions (shown in Figure 5a), which is taken into account by the color rendering index.

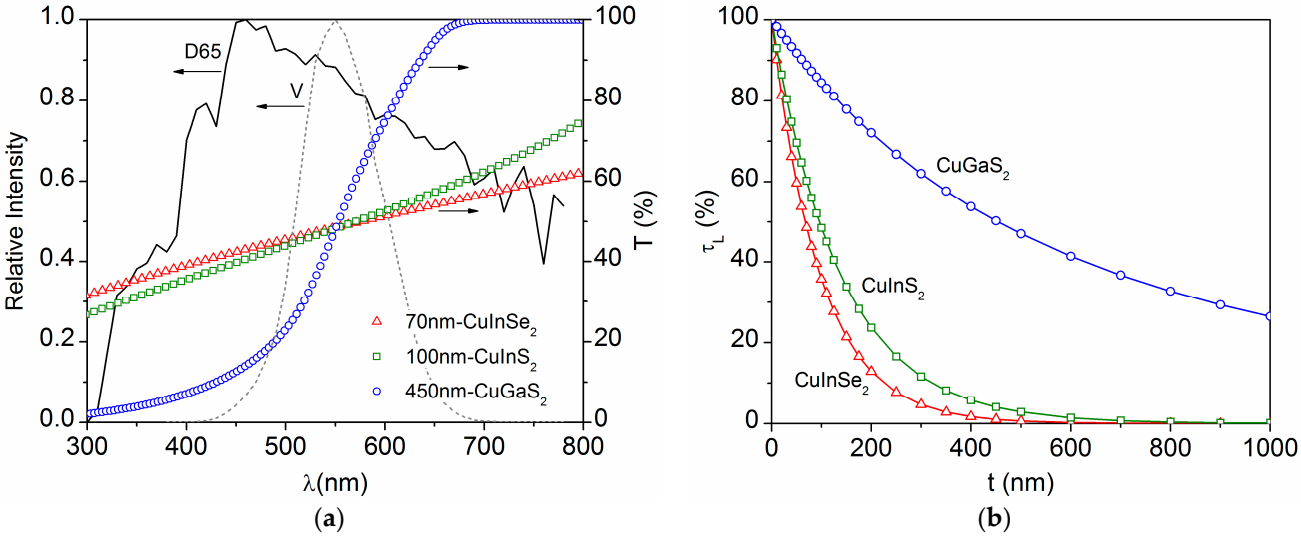

Figure 5. (**a**) Comparison of standard illuminant D65 and standard photopic vision V with the spectral transmittance of various chalcopyrite films with τ_L = 50%, and (**b**) luminous transmittance for each chalcopyrite compound as a function of its thickness.

Figure 6a depicts the evolution of the average color rendering index, R_a, calculated using Equation (19), and the correlated color temperature, CCT, calculated using Equation (9), depending on the chalcopyrite film thickness. An analogous behavior is observed for these parameters, both decreasing as the film thickness increases, and similar values are observed for the three chalcopyrite compounds, despite their different luminous transmittances. In fact, for a given thickness, R_a and CCT are found to be slightly higher for $CuInSe_2$ and $CuInS_2$ than for $CuGaS_2$, contrary to their respective τ_L values shown in Figure 5b. This is because not only a higher transmittance but also smoother variations in the visible range provide better color rendering [35]. According to the criteria for semitransparent glazing [19], a good index $R_a \geq 60\%$ is obtained for the various chalcopyrite compounds with thickness $t \leq 250$ nm, and an excellent $R_a \geq 80\%$ is obtained for $t \leq 130$ nm. Regarding the color temperature of the transmitted light, the values CCT > 3000 K for $t \leq 400$ nm are considered suitable for visual comfort [36]. The correlation of CCT and R_a is illustrated in Figure 6b, where the data obtained for the different chalcopyrite films follow a parabolic relationship: $R_a = -3.3 \cdot 10^{-6}CCT^2 + 0.05CCT - 85$. Some authors report a linear fit $R_a = 0.017CCT$ for dye sensitized solar cells, although only in the range of 3500 K < CCT < 5500 K. Figure 6b shows that the linear relationship also applies to the chalcopyrite data in a short CCT region, but R_a decreases quickly for CCT < 3500 K, as observed for other semitransparent devices [37].

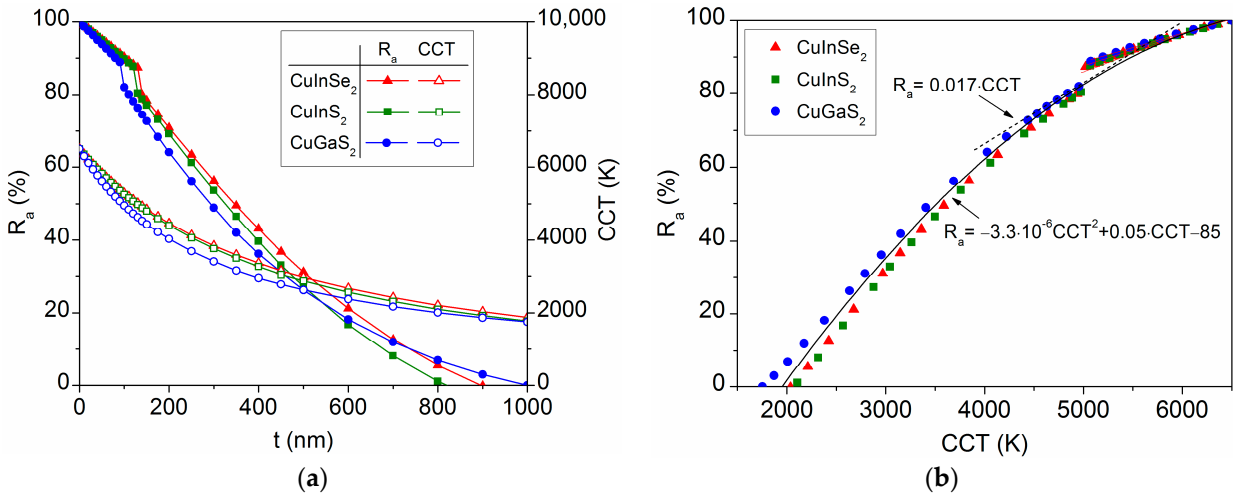

Figure 6. (**a**) Average color rendering index (R_a) and correlated color temperature obtained for each chalcopyrite compound as a function of the film thickness, and (**b**) connection between the respective R_a and CCT values, showing a linear fit over a small CCT range (dashed line) and a parabolic fit over the whole CCT range (solid line).

In order to better evaluate these chalcopyrite materials for application in semitransparent solar cells, a figure of merit can be defined as the product of the solar absorptance and luminous transmittance:

$$\phi_L = \alpha_S \tau_L \quad (22)$$

which is analogous to the light utilization efficiency used for photovoltaic devices [18,35], but replacing the conversion efficiency with α_S to consider only the absorber material. Furthermore, to take into account the color rendering, it is interesting to define another figure of merit in the form:

$$\phi_{La} = \alpha_S \tau_L R_a \quad (23)$$

which includes the two optical parameters (τ_L and R_a) that describe the visual comfort. Figure 7 presents both ϕ_L and ϕ_{La} for the various chalcopyrite compounds as a function of the film thickness. The best results are obtained for $CuInSe_2$ (with maximum ϕ_L = 18% and ϕ_{La} = 17% for t = 70 ± 20 nm), followed by $CuInS_2$ (maximum ϕ_L = 15% and ϕ_{La} = 14% for

t = 90 ± 30 nm) and $CuGaS_2$ (with maximum ϕ_L = 13% for t = 350 ± 100 nm and maximum ϕ_{La} = 8% for t = 180 ± 50 nm). The difference between ϕ_L and ϕ_{La} is larger for $CuGaS_2$ due to its relatively lower R_a index. In addition, it should be noted that all three compounds give the same value ϕ_{La} = 8% for t~180 nm, but $CuInSe_2$ and $CuInS_2$ can achieve higher ϕ_{La} with a lower thickness, requiring less material consumption and reduced deposition time as additional advantages. For semitransparent solar cells, an absorber layer as thin as 30 nm has been reported [13].

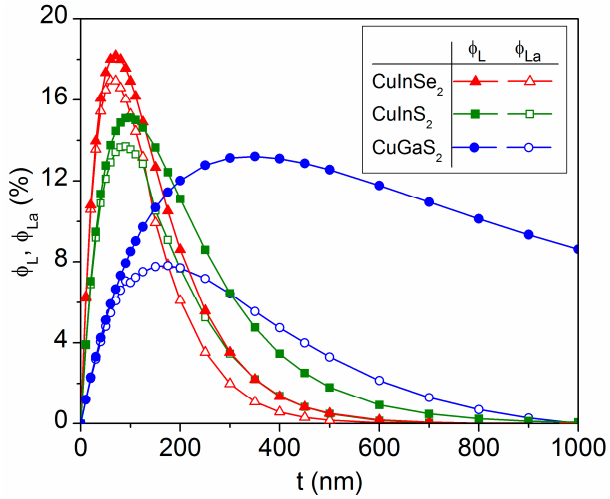

Figure 7. Figures of merit, $\phi_L = \alpha_S \tau_L$ and $\phi_{La} = \alpha_S \tau_L R_a$, for the chalcopyrite $CuInSe_2$, $CuInS_2$ and $CuGaS_2$ thin films as a function of the respective thickness.

4. Conclusions

The evaporated chalcopyrite thin films have shown high optical absorption coefficients below the respective gap wavelength ($\alpha > 10^4$ cm^{-1} at $\lambda < \lambda_g$), which increases from λ_g = 560 nm for $CuGaS_2$ to λ_g = 870 nm for $CuInS_2$ and λ_g = 1220 nm for $CuInSe_2$, with some additional absorption slightly above λ_g due to band tails. The experimental coefficients obtained for each chalcopyrite compound provide absorptance and transmittance spectra that depend on the film thickness and allow a comparative analysis of the solar absorptance, luminous transmittance and color rendering index. Regarding the correlated color temperature of the transmitted light, also considered as a factor for visual comfort, it is directly related to the color rendering index through a parabolic relationship.

According to the criteria for semitransparent glazing, a good index $R_a \geq 60\%$ (CCT ≥ 4000 K) is obtained for the three chalcopyrite compounds with thickness t ≤ 250 nm, and an excellent $R_a \geq 80\%$ (CCT ≥ 4800 K) is obtained for t ≤ 130 nm. For a given thickness, R_a is slightly higher for $CuInSe_2$ and $CuInS_2$ than for $CuGaS_2$, contrary to their respective τ_L values, due to the smoother variation of $CuInSe_2$ and $CuInS_2$ transmittances in the visible region. Otherwise, the absorbed solar irradiance increases with the film thickness faster for $CuInSe_2$ and $CuInS_2$ than for $CuGaS_2$.

The product of the solar absorptance, luminous transmittance and color rendering index is considered here as a new figure of merit, $\phi_{La} = \alpha_S \tau_L R_a$, to evaluate these absorber materials for their incorporation into semitransparent solar cells. Applying this quantification, the best result corresponds to $CuInSe_2$ (with maximum ϕ_{La} = 17% for t = 70 ± 20 nm), followed by $CuInS_2$ (maximum ϕ_{La} = 14% for t = 90 ± 30 nm) and $CuGaS_2$ (maximum ϕ_{La} = 8% for t = 180 ± 50 nm). These data provide guidelines for the design of semitransparent photovoltaic devices based on chalcopyrite absorbers.

Funding: This research received no external funding.

Data Availability Statement: The original contributions presented in the study are included in the article, further inquiries can be directed to the corresponding author.

Conflicts of Interest: The author declares no conflicts of interest.

References

1. Kumar, P.; You, S.; Vomiero, A. Recent progress in materials and device design for semitransparent photovoltaic technologies. *Adv. Energy Mater.* **2023**, *13*, 2301555. [CrossRef]
2. Shin, M.J.; Jo, J.H.; Cho, A.; Gwak, J.; Yun, J.H.; Kim, K.; Ahn, S.K.; Park, J.H.; Yoo, J.; Jeong, I.; et al. Semi-transparent photovoltaics using ultra-thin Cu(In,Ga)Se_2 absorber layers prepared by single-stage co-evaporation. *Sol. Energy* **2019**, *181*, 276–284. [CrossRef]
3. Chae, Y.T.; Kim, J.; Park, H.; Shin, B. Building energy performance evaluation of building integrated photovoltaic (BIPV) window with semi-transparent solar cells. *Appl. Energy* **2014**, *129*, 217–227. [CrossRef]
4. Chee, A.K.W. On current technology for light absorber materials used in highly efficient industrial solar cells. *Renew. Sustain. Energy Rev.* **2023**, *173*, 113027. [CrossRef]
5. Sivaraj, S.; Rathanasamy, R.; Kaliyannan, G.V.; Panchal, H.; Jawad Alrubaie, A.; Musa Jaber, M.; Said, Z.; Memon, S. A comprehensive review on current performance, challenges and progress in thin-film solar cells. *Energies* **2022**, *15*, 8688. [CrossRef]
6. Siebentritt, S.; Lomuscio, A.; Adeleye, D.; Sood, M.; Dwivedi, A. Sulfide chalcopyrite solar cells—Are they the same as selenides with a wider bandgap? *Phys. Status Solidi Rapid Res. Lett.* **2022**, *16*, 2200126. [CrossRef]
7. Kim, S.; Nagai, T.; Tampo, H.; Ishizuka, S.; Shibata, H. Large open-circuit voltage boosting of pure sulfide chalcopyrite Cu(In,Ga)S_2 prepared using Cu-deficient metal precursors. *Prog. Photovoltaics Res. Appl.* **2020**, *28*, 816–822. [CrossRef]
8. Klenk, R.; Klaer, J.; Scheer, R.; Lux-Steiner, M.C.; Luck, I.; Meyer, N.; Rühle, U. Solar cells based on $CuInS_2$—An overview. *Thin Solid Films* **2005**, *480–481*, 509–514. [CrossRef]
9. Qi, Y.; Liu, Q.; Tang, K.; Liang, Z.; Ren, Z.; Liu, X. Synthesis and characterization of nanostructured wurtzite $CuInS_2$: A new cation disordered polymorph of $CuInS_2$. *J. Phys. Chem. C* **2009**, *113*, 3939–3944. [CrossRef]
10. Gogova, D.; Olsen, V.S.; Bazioti, C.; Lee, I.H.; Prytz, Ø.; Vines, L.; Kuznetsov, A.Y. High electron mobility single-crystalline $ZnSnN_2$ on ZnO (0001) substrates. *CrystEngComm* **2020**, *22*, 6268–6274. [CrossRef]
11. Nezhdanov, A.; Skrylev, A.; Shestakov, D.; Usanov, D.; Fukina, D.; Malyshev, A.; De Filpo, G.; Mashin, A. Mixed phase $ZnSnN_2$ thin films for solar energy applications: Insight into optical and electrical properties. *Opt. Mater.* **2023**, *144*, 114335. [CrossRef]
12. Massiot, I.; Cattoni, A.; Collin, S. Progress and prospects for ultrathin solar cells. *Nat. Energy* **2020**, *5*, 959–972. [CrossRef]
13. Shin, M.J.; Lee, A.; Park, J.H.; Cho, A.; Ahn, S.K.; Shin, D.; Gwak, J.; Yun, J.H.; Yoo, J.; Cho, J.S. Ultrathin Cu(In,Ga)Se_2 transparent photovoltaics: An alternative to conventional solar energy-harvesting windows. *Nano Energy* **2022**, *92*, 106711. [CrossRef]
14. *EN 410:2011*; Glass in Building. Determination of Luminous and Solar Characteristics of Glazing. European Committee for Standardization: Bruxelles, Belgium, 2011.
15. *CIE 13.3:1995*; Method of Measuring and Specifying Colour Rendering Properties of Light Sources. International Commission on Illumination: Vienna, Austria, 1995.
16. Gueymard, C.A.; duPont, W.C. Spectral effects on the transmittance, solar heat gain, and performance rating of glazing systems. *Sol. Energy* **2009**, *83*, 940–953. [CrossRef]
17. Li, D.H.W.; Lam, T.N.T.; Chan, W.W.H.; Mak, A.H.L. Energy and cost analysis of semi-transparent photovoltaic in office buildings. *Appl. Energy* **2009**, *86*, 722–729. [CrossRef]
18. Traverse, C.J.; Pandey, R.; Barr, M.C.; Lunt, R.R. Emergence of highly transparent photovoltaics for distributed applications. *Nat. Energy* **2017**, *2*, 849–860. [CrossRef]
19. Ghosh, A.; Selvaraj, P.; Sundaram, S.; Mallick, T.K. The colour rendering index and correlated colour temperature of dye-sensitized solar cell for adaptive glazing application. *Sol. Energy* **2018**, *163*, 537–544. [CrossRef]
20. Lynn, N.; Mohanty, L.; Wittkopf, S. Color rendering properties of semi-transparent thin-film PV modules. *Build. Environ.* **2012**, *54*, 148–158. [CrossRef]
21. Martín-Chivelet, N.; Guillén, C.; Trigo, J.F.; Herrero, J.; Pérez, J.J.; Chenlo, F. Comparative performance of semi-transparent PV modules and electrochromic windows for improving energy efficiency in buildings. *Energies* **2018**, *11*, 1526. [CrossRef]
22. Guillén, C.; Herrero, J. $CuInS_2$ and $CuGaS_2$ thin films grown by modulated flux deposition with various Cu contents. *Phys. Status Solidi* **2006**, *203*, 2438–2443. [CrossRef]
23. Guillén, C. Evaporated chalcopyrite thin films for indoor photovoltaic applications. *Adv. Energy Convers. Mater.* **2024**, *5*, 31–39. [CrossRef]
24. Woods-Robinson, R.; Han, Y.; Zhang, H.; Ablekim, T.; Khan, I.; Persson, K.A.; Zakutayev, A. Wide band gap chalcogenide semiconductors. *Chem. Rev.* **2020**, *120*, 4007–4055. [CrossRef] [PubMed]
25. Kim, S.; Yoo, J.; Lee, M.; Jung, J.; Jang, J. $CuInSe_2$-based near-infrared photodetector. *Appl. Sci.* **2021**, *12*, 92. [CrossRef]
26. Dolgonos, A.; Mason, T.O.; Poeppelmeier, K.R. Direct optical band gap measurement in polycrystalline semiconductors: A critical look at the Tauc method. *J. Solid State Chem.* **2016**, *240*, 43–48. [CrossRef]
27. Bangolla, H.K.; Nallapureddy, R.R. MCSK Cu-rich copper indium sulfide thin films deposited by co-evaporation for photovoltaic applications. *J. Mater. Sci. Mater. Electron.* **2023**, *34*, 341. [CrossRef]
28. Wang, L.; Yuan, X.; Wang, Y.; Yao, W.; Zhu, J.; Jing, W. Preparation and characterization of $CuGaS_2$ thin films as a promising parent material for intermediate band solar cells. *Mater. Sci. Semicond. Process.* **2015**, *30*, 267–270. [CrossRef]

29. Nishiwaki, M.; Nagaya, K.; Kato, M.; Fujimoto, S.; Tampo, H.; Miyadera, T.; Chikamatsu, M.; Shibata, H.; Fujiwara, H. Tail state formation in solar cell materials: First principles analyses of zincblende, chalcopyrite, kesterite, and hybrid perovskite crystals. *Phys. Rev. Mater.* **2018**, *2*, 1–28. [CrossRef]
30. Katahara, J.K.; Hillhouse, H.W. Quasi-Fermi level splitting and sub-bandgap absorptivity from semiconductor photoluminescence. *J. Appl. Phys.* **2014**, *116*, 173504. [CrossRef]
31. Sritrakool, W.; Sa-yakanit, V.; Glyde, H.R. Band tails in disordered systems. *Phys. Rev. B* **1986**, *33*, 1199–1202. [CrossRef]
32. Rey, G.; Larramona, G.; Bourdais, S.; Choné, C.; Delatouche, B.; Jacob, A.; Dennler, G.; Siebentritt, S. On the origin of band-tails in kesterite. *Sol. Energy Mater. Sol. Cells* **2018**, *179*, 142–151. [CrossRef]
33. Kruse, O.; Rupprecht, J.; Mussgnug, J.H.; Dismukes, G.C.; Hankamer, B. Photosynthesis: A blueprint for solar energy capture and biohydrogen production technologies. *Photochem. Photobiol. Sci.* **2005**, *4*, 957–970. [CrossRef]
34. Venkateswararao, A.; Ho, J.K.W.; So, S.K.; Liu, S.W.; Wong, K.T. Device characteristics and material developments of indoor photovoltaic devices. *Mater. Sci. Eng. R Rep.* **2020**, *139*, 100517. [CrossRef]
35. Meddeb, H.; Götz-Köhler, M.; Neugebohrn, N.; Banik, U.; Osterthun, N.; Sergeev, O.; Berends, D.; Lattyak, C.; Gehrke, K.; Vehse, M. Tunable photovoltaics: Adapting solar cell technologies to versatile applications. *Adv. Energy Mater.* **2022**, *12*, 2200713. [CrossRef]
36. Nundy, S.; Mesloub, A.; Alsolami, B.M.; Ghosh, A. Electrically actuated visible and near-infrared regulating switchable smart window for energy positive building: A review. *J. Clean. Prod.* **2021**, *301*, 126854. [CrossRef]
37. Ghosh, A.; Mesloub, A.; Touahmia, M.; Ajmi, M. Visual comfort analysis of semi-transparent perovskite based building integrated photovoltaic window for hot desert climate (Riyadh, Saudi Arabia). *Energies* **2021**, *14*, 1043. [CrossRef]